Journal of Systems Engineering and Electronics
Vol. 37, No. 3, June 2026, pp.1030 – 1041

SINS/RCNS integrated navigation method based on LSTM algorithm for aerospace vehicle

YANG Shuning, WANG Dingjie, ZHANG Hongbo, and TANG Guojian*

College of Aerospace Science, National University of Defense Technology, Changsha 410073, China

Abstract: We propose a deep-learning-assisted strapdown inertial navigation system (SINS)/refraction celestial navigation system (RCNS) integrated navigation method to control the adverse effects of atmospheric density errors on the accuracy of stellar refraction navigation and enhance the reliability of SINS/RCNS integrated navigation for aerospace vehicles. This method utilizes satellite navigation data and a long short-term memory network to establish a mapping relationship between the navigation moments, refraction angles, and the apparent height errors. Using deep learning algorithm to address complex time-series prediction problems, thereby compensates the impact of atmospheric density deviations on star sensor measurements. Simulation experiments of vehicle navigation in scenarios with atmospheric density errors are conducted using this method. The results show that the deep learning scheme can effectively resist the adverse effects of atmospheric density errors on navigation, demonstrating strong reliability.

Keywords: deep learning, long short-term memory (LSTM) network, stellar refraction navigation, atmospheric density error, inertial navigation.

DOI: 10.23919/JSEE.2026.000054

1. Introduction

Aerospace vehicles rely on navigation systems to provide three-dimensional position, velocity, and attitude information during maneuvers. High-precision autonomous navigation is a prerequisite for aerospace applications. Strapdown inertial navigation system (SINS), which is one of the most commonly used navigation methods for aircraft, offers high service frequency and good continuity [1], whereas celestial navigation, as a completely autonomous method, uses stars for positioning and orientation, and does not accumulate errors, which compensates for the increasing error of inertial navigation over time [2]. The complementary advantages of these two methods enable the inertial/celestial integrated navigation approach to provide stable navigation information without external signals, thereby ensuring the navigation accuracy of long-endurance vehicles [3–5].

However, in practical applications, errors in atmospheric density models are key factors that limit the accuracy of refraction celestial navigation system (RCNS) for aerospace vehicles [6]. Significant errors in atmospheric density can severely degrade the forecast accuracy of the stellar refraction angle model, leading to an incorrect estimation of navigation error states and undermining the precision level [7,8]. Current methods for combating navigation failures caused by inaccurate atmospheric density primarily focus on two aspects: improving the stellar atmospheric refraction model, navigation error estimation and compensation [9]. For model optimization, Mai et al. [10] proposed an atmospheric refraction prediction method based on an improved extreme gradient boosting algorithm, using a comprehensive learning particle swarm optimization algorithm to enhance the accuracy of the atmospheric refraction model. Wu et al. [11] constructed a stellar atmospheric refraction model based on the geometric ray tracing law using a back propagation (BP) neural network to more accurately describe the relationship between time, position, and refraction angle. Peng et al. [12] proposed a spatiotemporal atmospheric refraction model correction method based on globally measured data, significantly improving the positioning accuracy under high-viewing-angle conditions by stratifying the atmosphere. Yang et al. [13] studied an adaptive atmospheric temperature and density model based on National Centers for Environmental Prediction (NCEP) atmospheric data to achieve high-precision navigation under complex atmospheric conditions through Fourier interpolation fitting. To improve the performance of SINS/RCNS integrated navigation systems further, many scholars conducted studies on estimation and compensation algorithms for atmospheric density errors [14–17]. Zhao et al. [18] proposed a tightly coupled SINS/RCNS inte-

Manuscript received September 06, 2024.
*Corresponding author.

grated navigation method that improved the accuracy of the navigation system by estimating and compensating for atmospheric density errors in real time. Gao et al. [19] proposed an integrated navigation method based on inertial/triple star sensors and deeply coupled stellar refraction navigation, which weakened the adverse effects of inaccurate atmospheric refraction models by dynamically adjusting the star measurement model. Xie et al. [20] established a refraction model considering refraction errors and imaging noise, and proposed a method for simultaneously estimating the atmospheric refraction of starlight and the attitude error of the star sensor, significantly reducing the measurement error of the navigation system.

Due to the complex and variable nature of atmospheric density influenced by multiple factors, the aforementioned model correction and error compensation methods struggle to overcome navigation failures caused by atmospheric density changes under complex environmental conditions, and room for further improvement in navigation accuracy still exists. With the further expansion of the research field, neural networks are applied to some extent in the field of navigation [21–24]. Deep-learning algorithms, with their largescale data processing capabilities and good adaptability, can make reasonable decisions based on current inputs and historical information [25–27]. High-quality historical data are key to effectively train a deep neural network. Global navigation satellite system (GNSS) can provide high precision navigation information throughout the day and night [28]. However, due to its susceptibility to interference and deception [29], GNSS has certain limitations in aerospace vehicle applications. However, when the electromagnetic environment is stable, the GNSS receivers can still be turned on for a certain period to accurately calculate the navigation information of the vehicle. Inspired by this, this paper proposes a method to roughly identify atmospheric density bias based on GNSS data, and a deep neural network assisted method to counteract the adverse effects of inaccurate atmospheric density models on the accuracy of SINS/RCNS integrated navigation for aerospace vehicles. The main contributions of this paper are as follows:

(i) A GNSS-assisted atmospheric density bias rough identification method is proposed. Based on the exponential model, the atmospheric density is represented as a coefficient form of the theoretical model. The atmospheric density error coefficient is roughly identified using the GNSS positioning results, and the atmospheric density error of the stellar refraction navigation is compensated.

(ii) A deep learning assisted SINS/RCNS integrated navigation method is proposed. This method uses GNSS data to train a deep neural network during the initial flight phase of a vehicle. When the GNSS stops working, a well-trained network is called to forecast the correction of the apparent height measurement of RCNS, ensuring that the measurement information is accurate and available, and maintain the precision and reliability of the integrated navigation system.

Compared to the traditional BP neural network algorithm, the simulation results show that our proposed deep learning assisted navigation algorithm can significantly compensate for errors in atmospheric density, offering higher navigation accuracy and providing a new approach for the robust navigation of aircraft in adverse atmospheric conditions.

The remainder of this paper is organized as follows. Section 2 introduces the integrated navigation system model. Section 3 introduces the impact of atmospheric density bias on RCNS and the method to roughly identify atmospheric density errors using GNSS data. Section 4 introduces the SINS/RCNS integrated navigation method based on deep learning algorithm. Section 5 presents the verification of the simulation experiment, and Section 6 presents the conclusions.

2. SINS/RCNS integrated navigation model

2.1 SINS dynamics model

In the geocentric inertial coordinate system, the basic equation for SINS can be expressed as follows:

$$\begin{cases} \dot{\boldsymbol{C}}_i^b = -\left[\boldsymbol{\omega}_{ib}^b \times\right] \boldsymbol{C}_i^b \\ \dot{\boldsymbol{v}}^i = \boldsymbol{C}_b^i \boldsymbol{f}^b + \boldsymbol{g}^i \\ \dot{\boldsymbol{r}}^i = \boldsymbol{v}^i \end{cases} \tag{1}$$

where $\boldsymbol{r}^i$ and $\boldsymbol{v}^i$ represent the position and velocity vectors, respectively in the inertial frame. $\boldsymbol{C}_i^b$ represents the transformation matrix. $\boldsymbol{\omega}_{ib}^b$ is the angular rate vector. $\boldsymbol{f}^b$ refers to apparent acceleration. $\boldsymbol{g}^i$ represents the gravity vector.

Assuming that the perturbation consists of constant and random parts, the discrete form of the error propagation equation for SINS in the geocentric inertial system is as follows:

$$\begin{pmatrix} \delta \boldsymbol{r}_k^i \\ \delta \boldsymbol{v}_k^i \\ \boldsymbol{\theta}_k \\ \boldsymbol{b}_{f,k} \\ \boldsymbol{b}_{\omega,k} \end{pmatrix} = \boldsymbol{\Phi}_{k,k-1} \begin{pmatrix} \delta \boldsymbol{r}_{k-1}^i \\ \delta \boldsymbol{v}_{k-1}^i \\ \boldsymbol{\theta}_{k-1} \\ \boldsymbol{b}_{f,k-1} \\ \boldsymbol{b}_{\omega,k-1} \end{pmatrix} + \boldsymbol{\Gamma}_k \begin{pmatrix} \delta \boldsymbol{f}_k^b \\ \delta \boldsymbol{\omega}_{ib,k}^b \end{pmatrix} \tag{2}$$

where $\delta \boldsymbol{r}_k^i$ and $\delta \boldsymbol{v}_k^i$ represent the position and velocity errors of the inertial navigation system; $\boldsymbol{\theta}_k$ is the misalignment angle; $\boldsymbol{b}_f$ and $\boldsymbol{b}_\omega$ are the bias errors of the accelerometer and gyroscope, respectively; $\delta\boldsymbol{f}^b$ and $\delta\boldsymbol{\omega}_{ib}^b$ are the random noise of the accelerometer and gyroscope, respectively; $\boldsymbol{\Phi}_{k,k-1}$ is the state transition matrix from time $k-1$ to time k, and $\boldsymbol{\Gamma}_k$ is the noise transfer matrix of the system. The detailed expression is provided in [30].

According to the covariance propagation law, the covariance prediction equation of the system can be obtained as

$$\boldsymbol{P}_k = \boldsymbol{\Phi}_{k,k-1}\boldsymbol{P}_{k-1}\boldsymbol{\Phi}_{k,k-1}^{\mathrm{T}} + \boldsymbol{\Gamma}_k\boldsymbol{Q}_k\boldsymbol{\Gamma}_k^{\mathrm{T}} \tag{3}$$

where $\boldsymbol{Q}_k$ is the covariance matrix of the random measurement noise of the inertial measurement units.

2.2 Star sensor attitude measurement model

Using the misalignment angle information output from the star sensor as the measurement, the measurement equation is as follows:

$$\hat{\boldsymbol{\theta}} = -\boldsymbol{C}_b^s\boldsymbol{\theta} - \boldsymbol{\theta}_s + \boldsymbol{\varepsilon} \tag{4}$$

where $\hat{\boldsymbol{\theta}}$ represents the misalignment angle observed by the star sensor, $\boldsymbol{\theta}_s$ is the installation misalignment angle of the star sensor, $\boldsymbol{C}_b^s$ is the installation matrix of the star sensor relative to the inertial navigation system, and $\boldsymbol{\varepsilon}$ is the attitude determination error that can be selected based on experience using classical algorithms.

2.3 Stellar refraction apparent height measurement model

After identifying the star image point imaging information and performing refractive star detection, if a refracted star is found, the apparent height can be calculated using the stellar refraction model [31] according to the following equation:

$$\begin{aligned} h_a = {} & h_0 - H\cdot\ln R + \\ & H\cdot\ln\left[k(\lambda)\cdot\rho_0\cdot\sqrt{2\pi R_e/H}\right] + R\sqrt{H\cdot R_e/(2\pi)} \end{aligned} \tag{5}$$

where ρ_0 refers to atmospheric density, H is the height of the atmospheric density scale, R is the angle of refraction, h_0 refers to the reference density, $k(\lambda)$ is the dispersion parameter, R_e refers to the radius of earth.

Additionally, the relationship between the apparent height and the position of the star sensor is given by

$$\hat{h}_a = \sqrt{\boldsymbol{r}^{\mathrm{T}}\boldsymbol{r} - (\boldsymbol{e}'^{\mathrm{T}}\boldsymbol{r})^{\mathrm{T}}\boldsymbol{e}'^{\mathrm{T}}\boldsymbol{r}} - R_e \tag{6}$$

where $\boldsymbol{e}'$ is the direction vector of starlight after refraction.

The difference in the apparent height calculated by the stellar refraction model and star sensor position is taken as the measurement quantity, from which the measurement equation can be derived as

$$\delta h_a = h_a - \hat{h}_a = -\frac{(\boldsymbol{r}^i - \boldsymbol{e}'\boldsymbol{e}'^{\mathrm{T}}\boldsymbol{r}^i)^{\mathrm{T}}\delta\boldsymbol{r}^i}{\sqrt{\boldsymbol{r}^{i\mathrm{T}}\boldsymbol{r}^i - \boldsymbol{r}^{i\mathrm{T}}\boldsymbol{e}'\boldsymbol{e}'^{\mathrm{T}}\boldsymbol{r}^i}} + \upsilon_a \tag{7}$$

where h_a is the theoretical value of the apparent height, $\hat{h}_a$ is the apparent height calculated from (6), and υ_a is the random error of the apparent height caused by the atmospheric model and refraction angle errors.

3. GNSS-assisted atmospheric density error compensation method for RCNS

3.1 Impact of atmospheric density errors on the accuracy of RCNS

From the geometric relationship between the apparent height of the refracted star and the observation position, we can derive:

$$h_a = \sqrt{r^2 - u^2} + u\tan R - R_e \tag{8}$$

where $r = |\boldsymbol{r}|$, $\boldsymbol{r}$ denote the vehicle position vectors. $u = |\boldsymbol{u}| = |\boldsymbol{r}\cdot\boldsymbol{e}|$, $\boldsymbol{e}$ is the starlight direction vector before refraction.

By substituting (5) into (8) and differentiating, the position error can be expressed as

$$\begin{aligned} \mathrm{d}\sqrt{r^2 - u^2} = {} & H\cdot\mathrm{d}\rho_0/\rho_0 - H\cdot\mathrm{d}R/R - \\ & u\cdot\mathrm{d}R + (HR_e/(2\pi))^{1/2}\mathrm{d}R, \end{aligned} \tag{9}$$

which describes the relationship among the vehicle position error $\mathrm{d}\sqrt{r^2-u^2}$, refraction angle measurement error $\mathrm{d}R$, and density error $\mathrm{d}\rho_0$.

At a height of 25 km, according to the U.S. Standard Atmosphere:

$$\begin{cases} H = 6.366\ \mathrm{km} \\ \rho_0 = 40.084\ \mathrm{g/m^3} \\ R = 148.1'' \end{cases} \tag{10}$$

1% error in atmospheric density can cause a vehicle position error of about 63.7 m, while even the most accurate existing atmospheric models can have atmospheric density errors of around 5% in a certain area. Therefore, it is of great significance to conduct research on methods of stellar refraction navigation that resist atmospheric density errors.

3.2 Rough online identification method for atmospheric density error

As analyzed above, the apparent height can be calculated based on the refraction angle and atmospheric density according to the stellar refraction model. It can also be calculated based on the position of the vehicle through geometric relationships. When an error is present in the atmospheric density model, the apparent height calculated by stellar refraction model deviated from the true value, whereas that calculated by the geometric relationship is unaffected. Therefore, the magnitude of the atmospheric density error can be determined by the difference between the apparent heights obtained using the two different methods. As widely used sources of external measurement information, satellite navigation systems can continuously provide high-precision positioning information. It is assumed that the apparent height calculated by the GNSS positioning result is a theoretical value without error, so the error in the apparent height caused by atmospheric density can be obtained, thereby estimating the atmospheric density error.

Based on this concept, this subsection presents an online identification method for atmospheric density errors assisted by GNSS. In the early stage of the navigation of the vehicle, GNSS receiver and star sensor work simultaneously, recording the difference in apparent heights calculated by GNSS data and the stellar atmospheric model; after GNSS is turned off, the true atmospheric density is solved using the weighted least squares criterion to identify the atmospheric density error.

The coefficient of influence of all factors, except height, on the atmospheric density is denoted as

$$c = \frac{\rho}{\rho_0} \tag{11}$$

where ρ is the actual atmospheric density with an error. Here, the apparent height can be calculated as

$$\tilde{h}_a = h_0 - H\ln R + H\cdot \ln[k(\lambda)\cdot c\cdot \rho_0\sqrt{2\pi R_e/H}] + R\cdot\sqrt{HR_e/(2\pi)}. \tag{12}$$

Combining (5) and (12), the apparent height error due to the atmospheric density error is expressed as

$$\delta h_{ac} = \tilde{h}_a - h_a = H\ln c. \tag{13}$$

The theoretical value of the apparent height can also be calculated from the GNSS positioning result according to (6). Substituting (12) and (6) into (13), when the GNSS stops working, according to the least squares method, the estimate of the atmospheric density coefficient c and its variance $\sum_c$ can be solved as

$$\begin{gathered}\ln\hat{c} = [\boldsymbol{W}H]^{-1}\boldsymbol{W}^{\mathrm{T}}\cdot\delta h_{ac}\\ \sum_c = \frac{\boldsymbol{R}_a}{H}\end{gathered} \tag{14}$$

where $\boldsymbol{W}$ is the weight matrix, and $\boldsymbol{W} = \boldsymbol{R}_a^{-1}$. $\boldsymbol{R}_a$ is the apparent height error-covariance matrix, which can be expressed as

$$\boldsymbol{R}_a = \left(\sqrt{\frac{HR_e}{2\pi}} - \frac{H}{R}\right)^2 \boldsymbol{R}_r \tag{15}$$

where $\boldsymbol{R}_r$ represents the refraction angle noise variance matrix.

Once the atmospheric density coefficient is estimated, the true atmospheric density can be calculated. Thereby the true value of the refracted apparent height is obtained, ensuring the accuracy of RCNS measurements.

4. Deep learning assisted SINS/RCNS integrated navigation method

In Section 3, we estimate the atmospheric density coefficient using GNSS data and calibrate the density error online. However, the atmospheric density error coefficient is not always constant, and may contain random noise. When the GNSS stops operating over time, the accuracy of SINS/RCNS integrat navigation may deteriorate. Therefore, we employe an artificial inteligence method, specifically a long short-term memory (LSTM) network, to forecast the correction of the apparent height in RCNS, aimed to better overcome the impact of atmospheric density error fluctuations on the navigation system.

4.1 Design of LSTM network

The LSTM network is a variant of the traditional recurrent neural network (RNN), which adds three “gates” to the hidden layer neurons of the RNN, enabling it to better handle complex time series prediction problems. The structure of the LSTM model is shown in Fig. 1.

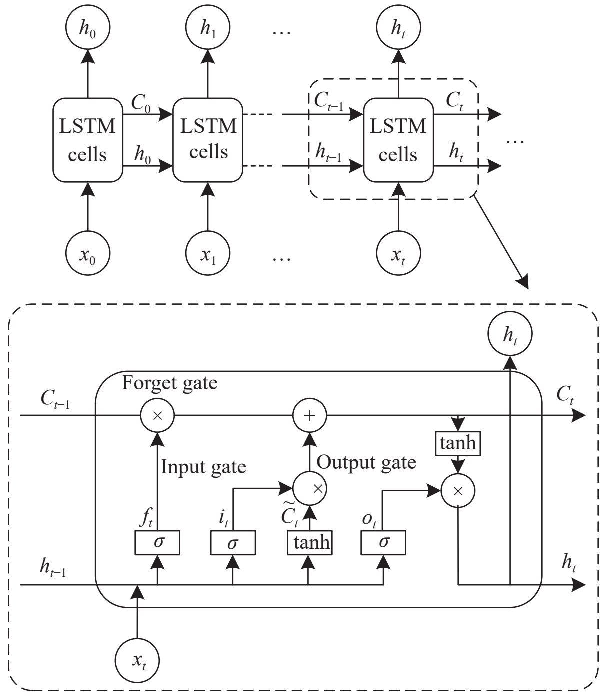

Fig. 1 LSTM model structure

The hidden units of the LSTM are used to store and transmit information, with three gates: the input gate, the output gate, and the forget gate. The forget gate determines the information that the memory cell needs to discard, the input gate decides the information that needs to be updated, and new information generated at this time is added to the memory cell to form new memory; finally, the output gate determines the information that the memory cell needs to output.

In this paper, an LSTM framework with eight layers is constructed to better predict time series. The network's hidden layers include two LSTM layers, one dropout layer, two fully connected layers, one rectified linear unit (ReLU) activation layer, and one huber regression layer. The specific training process is as follows:

(i) Network initialization. The LSTM network has two layers, containing 128 and 64 hidden units respectively; a dropout layer is used, which randomly disables neurons with a probability of 30% during each training to reduce the probability of model overfitting; in the regression layer, the huber loss function is used, which uses mean squared error (MSE) when the predicted value is close to the true value and mean absolute error (MAE) when it is far away, to reduce the impact of outliers on model training.

(ii) Dataset normalization. To eliminate the influence of different dimensions between data, the original time series dataset needs to be normalized using Min-Max normalization. The original dataset is $x=\{x_1,x_2,\cdots,x_n\}$, and the normalized dataset is $x'=\{x'_1,x'_2,\cdots,x'_n\}$, with the formula as follows:

$$x'=(x-x_{\min})(x_{\max}-x_{\min}). \tag{16}$$

(iii) Dataset division. After shuffling the data, it is divided into 80% training set and 20% test set.

(iv) Network training. The hyperparameters of the LSTM model and other settings are as follows:

i) Optimizer: The adaptive moment estimation (Adam) optimizer is chosen;

ii) Maximum number of iterations: 800;

iii) Learning rate: The initial learning rate is set to 0.001, with a piecewise learning rate adjustment strategy;

iv) Regularization parameter: The L2 regularization strength is set to 0.001 to control the model complexity and prevent overfitting;

v) Gradient clipping strategy: When the gradient value is greater than 5, clipping is performed to prevent gradient explosion.

(v) The output data p is de-normalized to obtain the final prediction result y, with the formula as follows:

$$y=p(x_{\max}-x_{\min})+x_{\text{mean}}. \tag{17}$$

4.2 SINS/RCNS navigation method based on LSTM network

The deep learning module based on the LSTM network consists of two working modes: the training update (as shown in Fig. 2) and forecasting (as shown in Fig. 3) modes. The network input includes the navigation moment of the observed refracted star T_k, the time interval of star observation $\Delta T_k=T_k-T_{k-1}$, the refraction angle R and refraction angle error δR; the network output is the correction of the apparent height at the corresponding moment $\delta h_{a,\text{RCNS}}$.

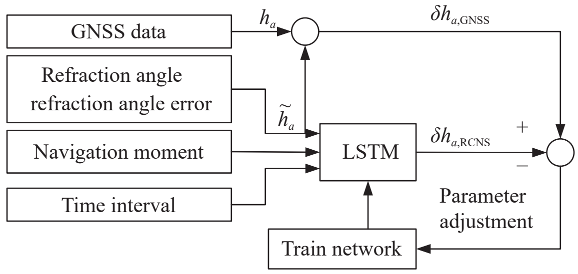

Fig. 2 Neural network training update mode system architecture

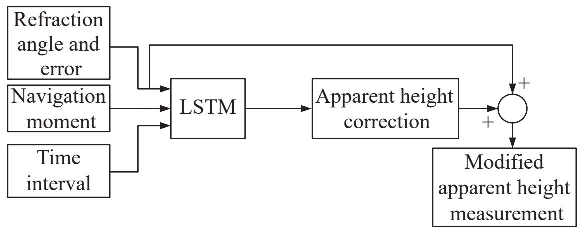

Fig. 3 Neural network forecasting mode system architecture

When GNSS signals are available, stellar refraction navigation does not participate in filtering, and the LSTM network operates in the training update mode. The training sample database records the current moment input data. Simultaneously, the apparent height h_a is calculated from the GNSS positioning results according to (6), and the difference is taken with the measured value of the apparent height $\tilde{h}_a$ output by the star sensor. The obtained difference $\delta h_{a,\text{GNSS}}$ is used as the target output of the neural network:

$$\delta h_{a,\text{GNSS}}=h_a-\tilde{h}_a. \tag{18}$$

When the GNSS is not operating, RCNS participates in filtering and corrects the SINS positioning error. At this time, the LSTM module switches to the forecasting mode to forecast the correction of the apparent height in stellar refraction navigation $\delta h_{a,\text{RCNS}}$, and then obtains the corrected refracted apparent height:

$$h_{a,\text{RCNS}}=\tilde{h}_a+\delta h_{a,\text{RCNS}}. \tag{19}$$

A well-trained neural network error model can forecast the apparent height error caused by the atmospheric density error at the current moment. This predicted error value is then used for RCNS apparent altitude correction. The method can accurately correct the apparent height error within a certain range of atmospheric density error fluctuations, thereby ensuring the reliability of the navigation system.

5. Experimental verification

5.1 Design of simulation experiment

A suborbital flight trajectory is generated to verify the effectiveness of the proposed algorithm. The designed simulation trajectory, velocity, and attitude information are shown in Fig. 4–Fig. 6. The initial launch position is 37°N and 97°E, and the coordinated universal time (UTC) corresponding to the launch is 1200 h on July 1, 2020, with a total flight time of 1462 s. The initial position, velocity, and attitude errors at launch are set to 200 m, 0.5°, and 0.1°, respectively.

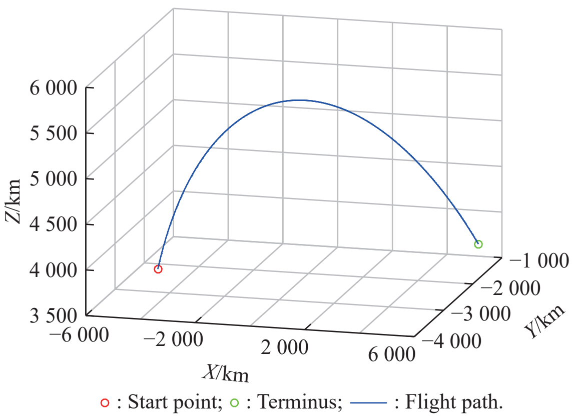

Fig. 4 Suborbital flight path

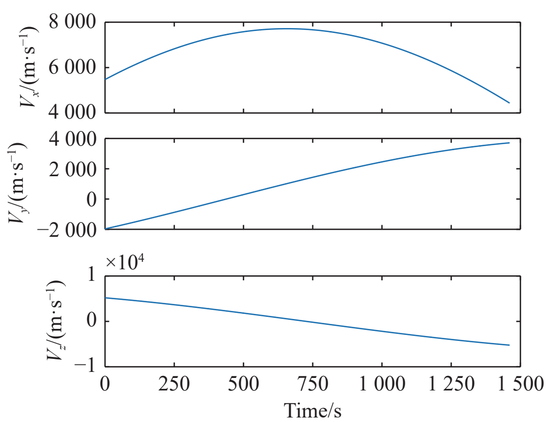

Fig. 5 Velocity change of the vehicle

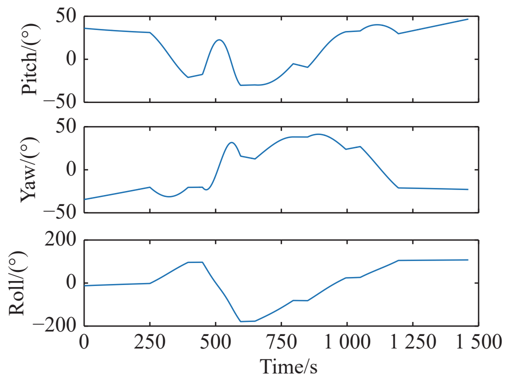

Fig. 6 Attitude change of the vehicle

Fig. 7 depicts the navigation scheme and the composition of the navigation system for aerospace vehicle. The parameters of the accelerometer, gyroscope, GNSS receiver, and star sensor used in the simulations are listed in Table 1. SINS is operated at a frequency of 200 Hz throughout the process. The star observation time periods of star sensor are set to [210, 250] s, [410, 450] s, [610, 650] s, [810, 850] s, [1010, 1050] s, and [1210, 1250] s, with a sampling frequency of 1 Hz, the rest of the flight time is used for other tasks such as maneuvering and attitude adjustment. GNSS receiver is turned on from 200 s to 650 s to identify atmospheric density errors or train the neural network.

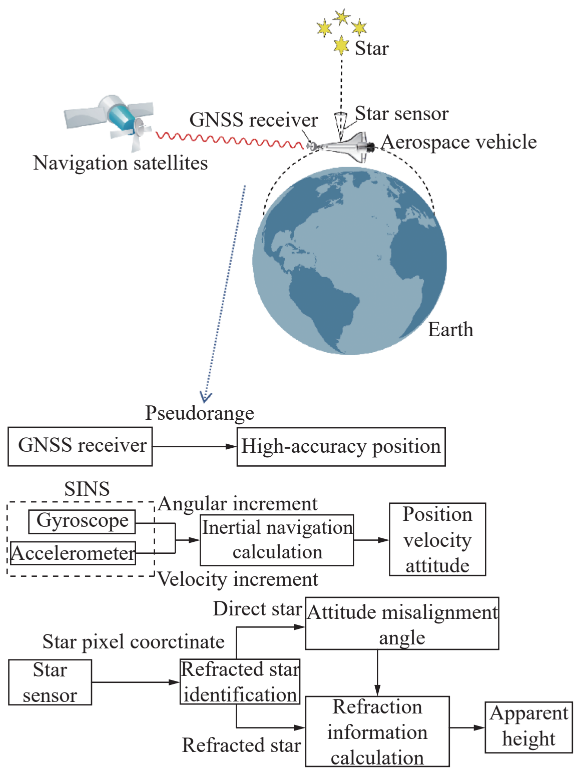

Fig. 7 Navigation scheme for aerospace vehicle

Table 1 Sensors simulation parameters

Device	Parameter	Value
SINS	Accelerometer bias	$1\times10^{-5}\,g$
	Accelerometer bias stability	$1\times10^{-5}\,g$
	Gyroscope bias/(°/h)	1×10^{-2}
	Gyroscope bias stability/(°/h)	5×10^{-3}
GNSS	Pseudo range/m	5
	Pseudo range variability/(m/s)	0.2
Star sensor	Field/(°)	12×12
	Pixel	1 024×1 024
	Installation misalignment angle accuracy/(″)	10
	Star pixel coordinate extraction accuracy/pixel	0.01

5.2 Analysis of the impact of atmospheric density errors on integrated navigation system

To verify the impact of atmospheric density errors on the accuracy of the SINS/RCNS integrated navigation, the GNSS receiver is turned off throughout the process, and 50 Monte Carlo targeting experiments are performed under the conditions of 0, 3%, and 10% atmospheric density errors. The results of the navigation root MSE (RMSE) at various flight moments are shown in Fig. 8.

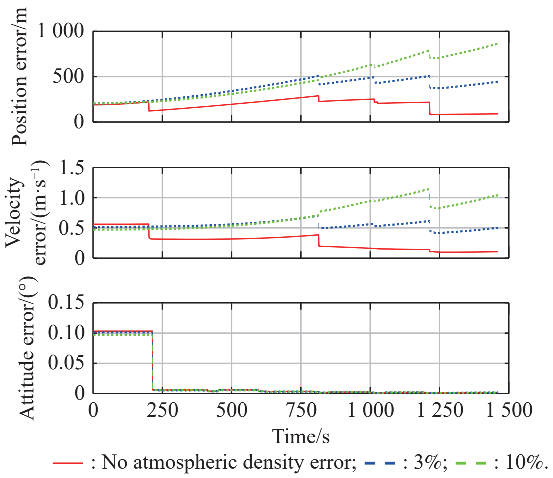

Fig. 8 Navigation accuracy under different atmospheric density error conditions

In Fig. 8, the red solid line represents the theoretical navigation accuracy under conditions with no atmospheric density bias; the blue and green dashed lines represent the navigation accuracy when the atmospheric density has errors of 3% and 10%, respectively. It can be seen from Fig. 8 that before 210 s, star sensor is not working, the three curves almost coincide, indicating that the integrated navigation system maintains a stable accuracy without the influence of atmospheric density errors. From 210 s, when the star sensor begins to work, the navigation error decreases when the refracted star is observed; the positioning and velocity accuracy curves of 10% and 3% atmospheric density errors exceed the accuracy curve without error, and the navigation error variances of 0, 3%, and 10% errors increase in turn. The navigation accuracies at the end of the statistical analyses are listed in Table 2. Fig. 8 and Table 2 show that atmospheric density errors have a non-negligible deteriorating effect on the positioning and velocity accuracy of SINS/RCNS integrated navigation, and the greater the atmospheric density error. Moreover, with the increase of the atmospheric density error, the greater the accuracy decreases. The attitude error curve shows that under the three atmospheric density conditions, the attitude accuracy does not change significantly, indicating that atmospheric density errors have little effect on attitude.

Table 2 Navigation accuracy at the endpoint

Error	Positioning/m	Velocity/(m/s)	Attitude/(″)
No error	89.75	0.11	6.28
3% error	444.20	0.50	5.74
10% error	863.71	1.04	6.34

5.3 Analysis of integrated navigation results without atmospheric density error compensation

A random constant error of 1%−10% is incorporated into the atmospheric density model. Fig. 9 presents a single experiment showing the position, velocity, and attitude estimation error curves obtained using the SINS/RCNS integrated navigation method without atmospheric density error correction.

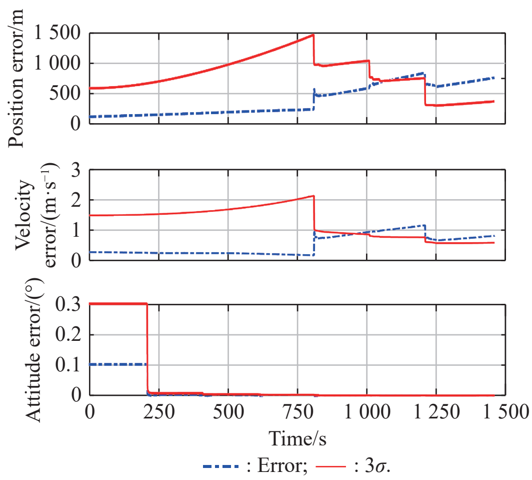

Fig. 9 Navigation error without atmospheric density error correction

The dark blue dashed line in Fig. 9 represents the navigation error curve, and the red solid line represents three times the theoretical error standard deviation line (3σ).

Fig. 9 shows that the SINS navigation error diverges slowly, and at 200 s, when the star sensor starts working, the celestial navigation system corrects the vehicle attitude error. Before 810 s, the navigation error is always below the 3σ line, indicating that the navigation system works normally when RCNS does not participate in filtering. Starting from 810 s, RCNS participates in filtering, the positioning and velocity error curves show a sudden increase and gradually diverge, exceeding the 3σ line. The endpoint positioning error reaches 770.30 m, and the velocity error is 0.83 m/s, indicating that atmospheric density errors severely affect the positioning and velocity accuracy of the navigation system, leading to filter divergence. Observing the attitude error curve, when the star sensor observes stars, the attitude theoretical 3σ line decreases, and throughout the operation of the navigation system, no case of attitude error exceeding the line exists, which is consistent with the above statement that atmospheric density errors have no significant deterioration effect on attitude.

5.4 Analysis of GNSS-assisted atmospheric density error rough compensation experiment

To evaluate the effectiveness of the GNSS-assisted atmospheric density error rough identification algorithm, we set the atmospheric density error to a random constant of 1%−10% and apply the rough identification method to the SINS/RCNS integrated navigation system. The position, velocity, and attitude estimation errors obtained from 100 Monte Carlo targeting experiments are illustrated in Fig. 10.

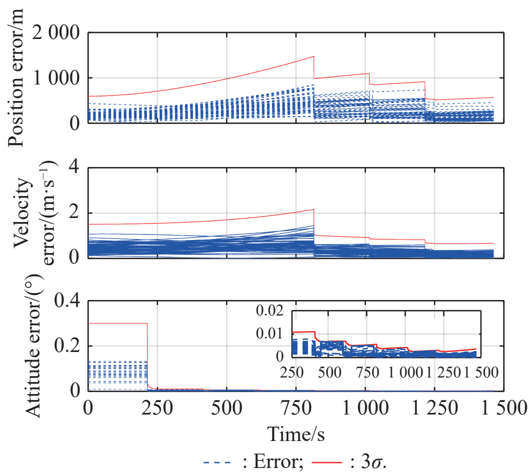

Fig. 10 Navigation error with rough identification method under constant atmospheric density error

In Fig. 10, each blue dashed line represents the navigation error obtained from the targeting experiment, and the red solid line represents the 3σ line. It is observed that throughout the operation of the integrated navigation system, the positioning and velocity errors are all below the 3σ line. Compared with Fig. 9, it can be stated that the identification and compensation algorithm proposed helps to resist atmospheric density errors and ensure the stability of the filter. Observing the positioning and velocity error curves in Fig. 10, it is found that at 810 s, 1010 s, and 1210 s, the theoretical 3σ line has a certain decline, indicating that when star sensor observes refracted stars, RCNS accurately corrects the positioning error. The RMSE of the navigation results at the end of the trajectory is 194.85 m for positioning, 0.21 m/s for velocity, and 6.48″ for attitude. Compared with the results without atmospheric density error correction, the navigation accuracy after compensation is significantly improved. The results show that the GNSS-assisted rough identification method is effective when the atmospheric density error is constant.

To further simulate the real atmospheric density error variations, the random noise ε and $\varepsilon \sim \mathrm{N}\left(0, 0.5^2\right)$ are added to the random constant error. The error curves of the position, velocity, and attitude estimation obtained by integrated navigation with the rough identification method are shown in Fig. 11.

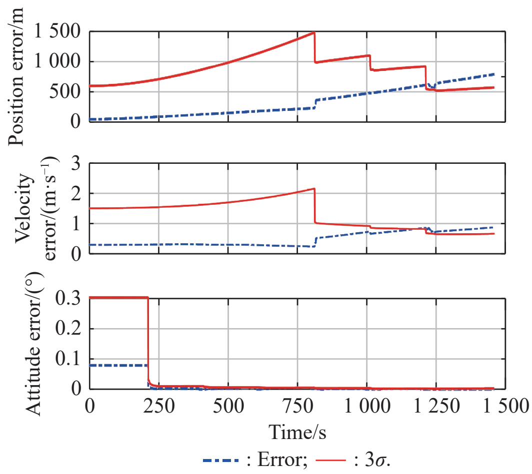

Fig. 11 Navigation error with rough identification method under fluctuating atmospheric density error

In Fig. 11, starting from 810 s, the blue dashed line indicates a sudden increase in the positioning and velocity errors, and the filter eventually diverges. This indicates that stellar refraction navigation makes incorrect corrections to the inertial navigation errors, leading to navigation failure. This shows that when the atmospheric density error fluctuates, the accuracy of the GNSS-assisted rough identification method is insufficient, deep learning methods are needed to further resist failures and ensure the navigation accuracy.

5.5 Experimental validation of deep learning-assisted SINS/RCNS integrated navigation method

To verify the effectiveness of the deep learning-assisted SINS/RCNS integrated navigation method, experiments are first conducted on the traditional BP neural network-assisted method, under the same noisy random constant atmospheric density error conditions as in the previous section; then, experiments on the LSTM-assisted method proposed in this paper is conducted; finally, the orbit is changed for experiments with deep learning methods to verify the generality of the approach.

Case 1 Traditional BP network-assisted SINS/RCNS integrated navigation method

In a particular experiment, the training results of the BP network are shown in Fig. 12.

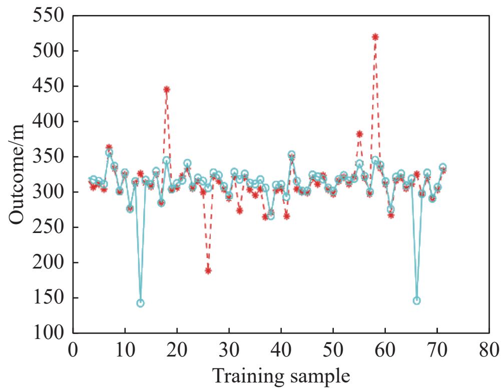

(a) Training set prediction results

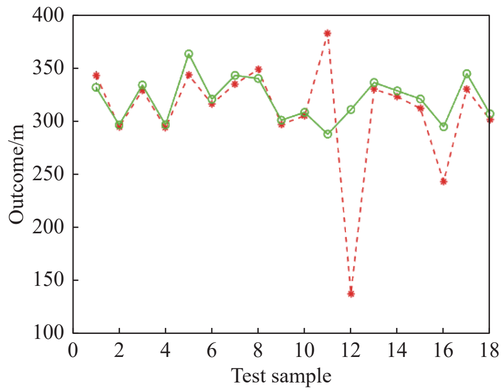

(b) Test set prediction results

: True value; : BP predicted results.

Fig. 12 BP network training results

In Fig. 12, the red solid line represents the theoretical values of the apparent height correction derived from GNSS data, while the blue dashed line and the green line represent the forecast results of the BP network's training and testing sets, respectively. The RMSE of the forecast for the testing set is statistically 42.68 m. Using the BP network forecast method, 100 Monte Carlo targeting experiments are conducted, and the position, velocity, and attitude estimation error curves obtained are shown in Fig. 13.

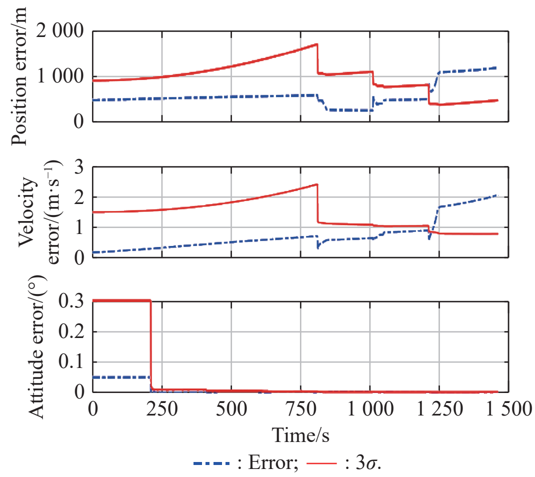

Fig. 13 Navigation error with BP network assistance under fluctuating atmospheric density error

From Fig. 13, it can be seen that during the observation period of [810, 850] s, the positioning and velocity errors represented by the blue dashed line show a reduction, indicating that the prediction results of the BP neural network successfully compensated for the errors in the atmospheric density model. However, in the observation periods of [1 010, 1 050] s and [1 210, 1 250] s, the error curves exhibit sudden changes, exceeding the theoretical 3σ threshold, demonstrating that the BP neural network predictions deviate from the true values, rendering the compensation method ineffective. These results indicate that traditional neural network approaches fail to ensure the reliability of navigation results, highlighting the necessity of employing deep learning methods.

Case 2 LSTM network-assisted SINS/RCNS integrated navigation method

In a particular experiment, the training results of the BP network are shown in Fig. 14.

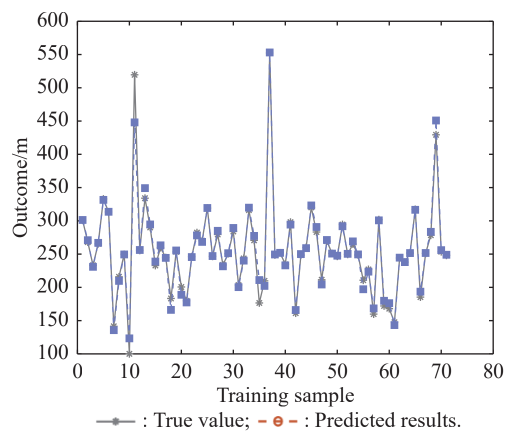

(a) Training set prediction results

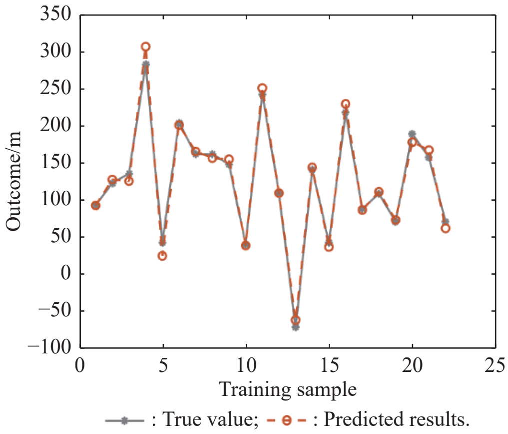

(b) Test set prediction results

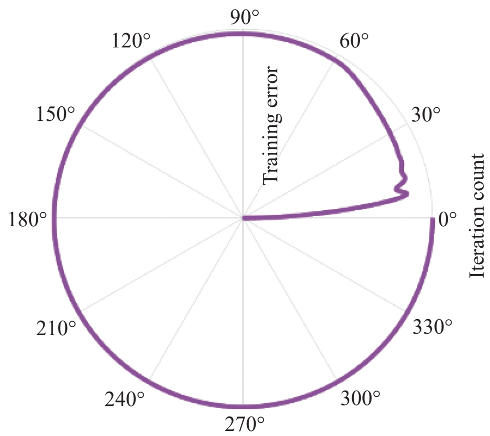

(c) Loss iteration curve

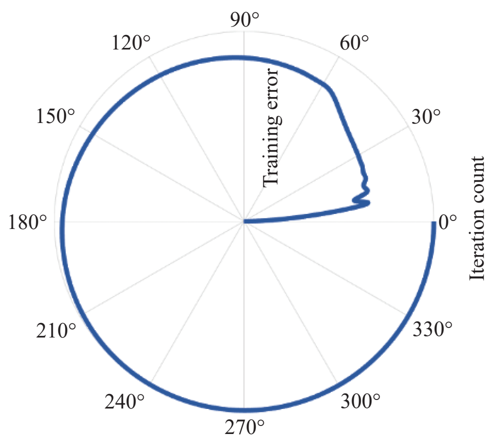

(d) RMSE iteration curve

Fig. 14 LSTM network training results

In Fig. 14(a) and Fig. 14(b), the gray solid line represents the theoretical values of the zenith delay corrections derived from GNSS data, while the blue and red lines represent the prediction results of the LSTM network for the training set and the test set, respectively. Fig. 14(c) and Fig. 14(d) show the convergence during the network training process. It can be observed from Fig. 14 that the network achieves good fitting accuracy and converges to a relatively small error. The prediction error statistics for the test set are as follows: the MAE is 6.96 m, the RMSE is 9.01 m, the mean absolute percentage error (MAPE) is 0.06, and the coefficient of determination (R^2) is 0.98. The network prediction method is used to conduct 100 Monte Carlo target-shooting experiments, and the error curves of the position, velocity, and attitude estimations obtained are shown in Fig. 15.

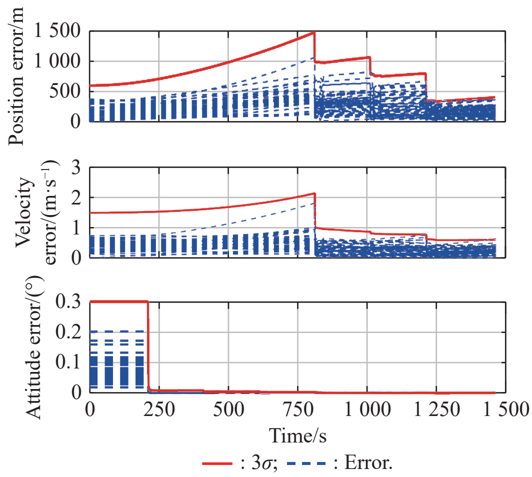

Fig. 15 Navigation error with deep learning assistance under fluctuating atmospheric density error

From Fig. 15, it can be seen that the positioning and velocity errors are all below the 3σ line, indicating that the navigation results are reasonable and effective. The RMSE at the end of the trajectory are 240.85 m for positioning, 0.28 m/s for velocity, and 6.95″ for attitude, indicating that the neural network correctly corrects the apparent height with errors. Compared with uncorrected methods, GNSS rough identification method and traditional BP network assisted method, the reliability of the deep learning aided method significantly improves under atmospheric density bias conditions.

Case 3 SINS/RCNS integrated navigation method assisted by LSTM network under different orbit

To verify the effectiveness and generalization ability of the deep learning method under different flight orbits, another spacecraft trajectory with different launch direction is generated, and the proposed method is used to compensate for the atmospheric density error. The initial position of the launch site is set at (34°N, 112°E), and the total flight time is 1 520 s. The initial position error, velocity error, and attitude error at launch are set to 300 m, 0.5 m/s, and 0.1°, respectively. The navigation sensor parameters are set as listed in Table 1. SINS operating at a frequency of 100 Hz throughout the flight. The star sensor observes the stars during three periods: [200, 250] s, [700, 750] s, and [1 200, 1 250] s, with a sampling frequency of 1 Hz. The satellite navigation receiver is active from 200 s to 250 s. In essence, the LSTM network predicts the apparent altitude correction during the periods of [700, 750] s and [1 200, 1 250] s. A total of 100 experiments are conducted, and the position, velocity, and attitude estimation error curves are shown in Fig. 16.

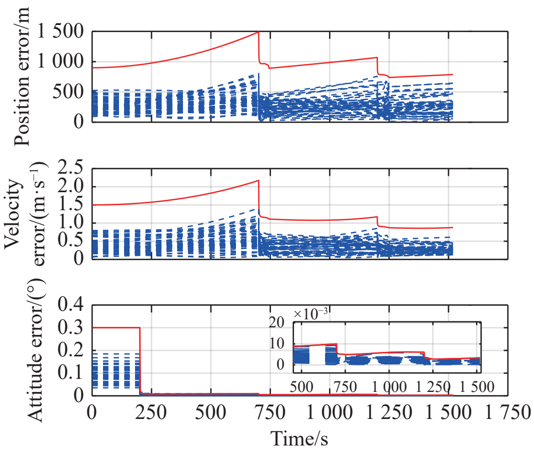

Fig. 16 Navigation error with deep learning assistance of medium Earth orbit spacecraft

In Fig. 16, each blue dashed line represents the navigation error obtained from a single experiment, while the red solid line represents the theoretical accuracy of 3σ. Throughout the operation of the integrated navigation system, no limit-exceeding phenomenon occurrs. Additionally, during the time periods of [700, 750] s and [1 200, 1 250] s, the positioning and velocity errors show a reduction, indicating that the LSTM network makes correct predictions for the altitude correction factor, overcoming the negative effects of atmospheric density errors. Simulations on different orbits demonstrate that the method of using deep learning to compensate for atmospheric density errors has a certain degree of generality.

6. Conclusions

To address the problem of atmospheric density error restricting the RCNS accuracy of spacecraft, a deep-learning-assisted SINS/RCNS integrated navigation method is proposed in this paper. This method makes use of the characteristics of LSTM dependent learning and the good generalization ability of long-term memory networks. It predicts the apparent height correction of RCNS based on GNSS positioning information, which can effectively correct the navigation deviation caused by atmospheric error and has good stability. Simulation results based on the typical orbit of a space vehicle show that when the atmospheric density error fluctuates, the proposed method can successfully suppress filter divergence. The navigation accuracy is better than that of the method that directly identifies errors through GNSS data or traditional BP neural networks. This method provides a new solution for integrated navigation of aerospace vehicles in harsh atmospheric environments. However, since the accuracy of deep learning methods cannot reach 100%, further exploration and solutions are needed to identify and suppress abnormal prediction results, ensuring the robustness of navigation.

References

[1] NING X L, YUAN W P, LIU Y H. A tightly coupled rotational SINS/CNS integrated navigation method for aircraft. Journal of Systems Engineering and Electronics, 2019, 30(3): 825–834.

[2] TANG J, BIAN H W. Ship SINS/CNS integrated navigation aided by LSTM attitude forecast. Journal of Marine Science and Engineering, 2024, 12(3): 389–403.

[3] SONG G X, YANG Y Q, NING X L, et al. A new SINS/RCNS integrated navigation method based on star pixel coordinates. Science China (Information Sciences), 2023, 66(9): 295–296.

[4] LIU B X, WEI S H, SU G H, et al. Key technologies and research status of midand long-range missile inertial/stellar integrated navigation system. Systems Engineering Theory and Practice, 2019, 39(5): 1351–1362. (in Chinese)

[5] CUI H, SHAO H B, ZHANG K. Inertial/stellar integrated navigation and simulation based on large-field-of-view star sensor. Computer Simulation, 2019, 36(1): 29–33, 56. (in Chinese)

[6] WU P F, SONG F, WEI H L. Research on atmospheric refraction model and data patterns for stellar navigation. Modern Defense Technology, 2017, 45(2): 6–13. (in Chinese)

[7] ZHAO Y, WANG D J, ZHANG H B, et al. A high-accuracy SINS/RCNS integrated navigation algorithm. Proc. of the Internal Conference on Guidance, Navigation and Control, 2022: 5508−5518.

[8] IFECHUKWU U N, TATA H, TIM O I. Assessment of GNSS zenith tropospheric delay responses to atmospheric variables derived from ERA5 data over Nigeria. Satellite Navigation, 2023, 4(1): 1–16.

[9] WANG X L, MA S. A celestial analytic positioning method by stellar horizon atmospheric refraction. Chinese Journal of Aeronautics. 2009, 22(3): 293–300.

[10] MAI Y B, SHENG Z, SHI H Q, et al. Using improved XGBoost algorithm to obtain modified atmospheric refractive index. International Journal of Antennas and Propagation, 2021, 2021(1): 1–11.

[11] WU S C, WANG H Y, WANG B W. Construction of a backpropagation starlight atmospheric refraction model based on ray tracing. Applied Optics, 2023, 62(14): 3778–3787.

[12] PENG X H, HUANG W W, LI X Y, et al. A spatiotemporal atmospheric refraction correction method for improving the geolocation accuracy of high-resolution remote sensing images. Remote Sensing, 2022, 14(21): 5344.

[13] YANG Y F, HAN X, SONG N N, et, al. A new method to improve the measurement accuracy of autonomous astronomical navigation. Journal of Mathematics, 2022, 2022: 3649662.

[14] ZHOU S T, ZHANG Q, GAO R. High accuracy atmospheric turbulence compensation based on a Wirtinger flow algo-

rithm in an orbital angular momentum free space optical communication system. Optics Communications, 2020, 477: 126322.

[15] YANG Y F, SONG N N, HAN X. Corrected starlight astmospheric refraction model based on NCEP database. Acta Optica Sinica, 2023, 43(18): 1801002.

[16] RATA J A, AMATO D, MC J W. Density estimation for entry guidance problems using deep learning. Proc. of the AIAA SCITECH 2024 Forum, 2024. DOI: 10.48550/arXiv.2310.19684.

[17] LI Y K, LIU C, WANG Y F, et al. A robust motion error estimation method based on raw data. IEEE Trans. on Geoscience and Remote Sensing, 2012, 50(7): 2780–2790.

[18] ZHAO Y, WANG D J, ZHANG H B, et al. A novel tightly-coupled SINS/RCNS integrated navigation method considering atmospheric density error. IEEE Trans. on Instrumentation and Measurement, 2023, 72: 1.

[19] GAO Z Q, WANG H Y, WANG W H, et al. SIMU/Triple star sensors integrated navigation method of HALE UAV based on atmospheric refraction correction. Journal of Navigation, 2022, 75(3): 704–726.

[20] XIE C T, JIANG J, YANG J S, et al. Simultaneous estimation of respective observation refraction and terrestrial star sensor attitude error. IEEE Trans. on Instrumentation and Measurement, 2023, 72: 5031512.

[21] JWO D J, BISWAL A, MIR I A. Artificial neural networks for navigation systems: a review of recent research. Applied Science, 2023, 13(7): 4475.

[22] BITAR N A, GAVRILOV A. A new method for compensating the errors of integrated navigation systems using artificial neural networks. Measurement: Journal of the International Measurement Confederation, 2021, 168: 108391.

[23] XU Y, WANG K, JIANG C H, et al. Motion-constrained GNSS/INS integrated navigation method based on BP neural network. Remote Sensing, 2022, 15: 154.

[24] ZHANG Z D, WU F L, LIU Y S, et al. A neural network aided integrated navigation algorithm based on vehicle motion mode information. Proc. of the IEEE International Conference on Signal Processing, Communications and Computing, 2019. DOI: 10.1109/ICSPC46631.2019.8960761.

[25] XIAO Y M, LUO H Y, ZHAO F, et al. Residual attention network-based confidence estimation algorithm for non-holonomic constraint in GNSS/INS integrated navigation system. IEEE Trans. on Vehicular Technology, 2021, 70(11): 11404–11418.

[26] ZHOU M, LUO J, VILLELLA J, et al. Large sequence models for sequential decision-making: a survey. Frontiers of Computer Science, 2023, 17(2): 345–367.

[27] HE Q Y, YU H P, LIANG D L, et al. Enhancing pure inertial navigation accuracy through a redundant high-precision accelerometer-based method utilizing neural networks. Sensors, 2024, 24(8): 2566.

[28] HE Y M, SCHUMANN J. A framework for the analysis of deep neural networks in autonomous aerospace applications using Bayesian statistics. Proc. of the IEEE Security and Privacy Workshops, 2020: 234–239.

[29] AKMAL R, ALEX M, FABIO D. Improving GNSS spoofing awareness in smartphones via statistical processing of raw measurements. IEEE Open Journal of the Communications Society, 2023, 4: 873–891.

[30] LU H F. Research on the key technology of integrated navigation based on inertial navigation, celestial navigation and ground-based pseudo-satellite navigation for automated transfer vehicle. Changsha: National University of Defense Technology, 2015. (in Chinese)

[31] YANG B, SI F, XU F, et al. Adaptive measurement model of navigation by stellar refraction based on multiple models switching. Journal of Navigation, 2014, 67(4): 673–685.